INVESTIGATING THE CONTROL OF SURFACE TEMPERATURE ON SURFACE RUGGEDNESS AT THE LUNAR POLES. Ariel N. Deutsch[1], Jennifer L. Heldmann[1], Anthony Colaprete[1], Kevin M. Cannon[2], and Richard C. Elphic[1], [1]NASA Ames Research Center, Mountain View, CA 94035, USA (adeutsch@usra.edu), [2]Colorado School of Mines, Golden, CO 80401, USA.

Introduction: Recent studies investigating the shallowing of polar craters with latitude suggest that tens of meters of ice-rich regolith may be present in the lunar subsurface [1, 2]. On Mars, the presence of ground ice is correlated with smooth surface textures, and subdued topography has helped provide insight into the distribution of martian ice [3–5]. Characterizing the surface texture of the lunar poles could similarly reveal important information on the distribution of sequestered ice, and is also important for characterizing surface traversability in preparation for ground operations.

Here we characterize surface texture by measuring the surface ruggedness within 12 polar craters (six at each pole). The investigated craters have large, flat floors that are divided into ices stability zones (ISZs, defined by $T_{max} \leq 112$ K [6]) and non-ISZs ($T_{max} > 112$ K). We analyze the relationship between surface ruggedness and surface temperature and discuss the possibility that polar ice is softening lunar topography within ISZs.

Methods: For each crater, we analyze the surface thermal environment using the average (T_{avg}) and maximum (T_{max}) surface temperatures measured with Diviner for north and south polar summer, representing the warmest local seasons [7]. We derive surface ruggedness within each crater where slopes are <10° from 20-, 40-, and 120-mpp DEMs using two quantities:

Terrain Ruggedness Index (TRI). A TRI represents the mean difference in elevation between a cell (i.e., a DEM pixel) and all directly adjacent cells [8]. A TRI is expressed as a distance measurement in meters.

Vector Ruggedness Measure (VRM). A VRM expresses ruggedness as the dispersion of vectors orthogonal to planar facets on a surface [9]. Slope and aspect are decomposed into 3-dimensional vector components as the resultant vector magnitude is calculated within a moving window (here, of 3×3 cells). VRM is a unitless measurement, ranging from 0 (no terrain variation) to 1 (complete terrain variation).

Results: The TRI and VRM reveal a bimodal distribution with respect to maximum surface temperature (**Fig. 1**) for each of the 12 analyzed craters. Both modes represent a clustering of locations where TRI and VRM are lower, indicating smoother surface textures. Mode 1 occurs at lower surface temperatures, where T_{max} is ≤ 112 K, coinciding with the temperature used to define ISZs. The location of Mode 2 is much more variable, reflective of each crater's individual thermal environment, and is generally centered at T_{max} between 170 and 235 K.

The location of Mode 1 is generally centered around T_{max} of ~95 K. Of the 12 craters analyzed, the only anomaly to this observation is Amundsen (**Fig. 1c, d**), whose first mode is centered around T_{max} of ~65 K.

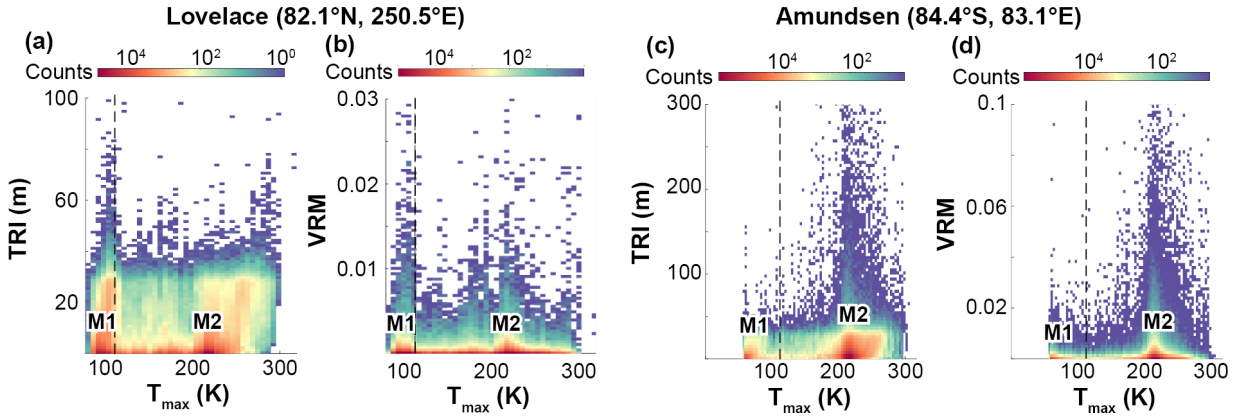

Fig. 1. Binned scatter plots display the relationships between texture indices and maximum surface temperature for (a, b) Lovelace and (c, d) Amundsen craters. The counts are plotted on a log scale. Modes 1 and 2 are labeled as M1 and M2 and the dashed vertical line in each subplot occurs at T_{max} = 112 K. The TRIs and VRMs were derived from DEMs with pixel resolutions of 20 m.

The individual modes are much more distinctive in T_{max} space than they are in T_{avg} space and often not resolvable in T_{avg} space, suggesting that T_{max} is the dominant temperature control on the location of smooth textures in polar ISZs.

Two-sample Kolmogorov-Smirnov tests indicate that the TRIs within ISZs and outside ISZs are not from the same continuous distribution ($\alpha = 0.05$). The mean and median TRIs are usually, but not always, lower within ISZs than they are outside ISZs. The difference in mean or median TRIs inside and outside of ISZs is typically only ~1 meter, indicating that there is not a substantial difference in ruggedness derived from 20-mpp DEMs using a moving window size of 3 cells.

Discussion: The distinct spatial correlation between ISZs and a clustering of smooth surface textures (Mode 1) as indicated by both TRIs and VRMs (**Fig. 1**) may be consistent with the presence of ice subduing surface topography.

Surface ice. There are various optical remote sensing data that suggest that thin frosts or diffuse ice mixed with the regolith may be present at the surface [e.g., 10–12] and previous work suggested that the presence of surface volatiles at the lunar poles is subduing surface roughness over ~50-m scales [13]. Specifically, Moon et al. found that "brightness roughness" derived from LROC optical images is lower in regions where surface ice is stable than it is in regions where either subsurface ice is stable or where no ice is stable [13].

Our study population includes both craters that do (N=7; e.g., **Fig. 1a, b**) and do not (N=5; e.g., **Fig. 1c, d**) host ice exposures derived from Moon Mineralogy Mapper (M^3) data [12]. Both populations show the same correlation between ISZs and smooth surface textures, suggesting that the surface ice detected using M^3 data is not the cause of the observed subdued topography in these regions. If surface ice *is* present in all of the investigated craters (N=12), then perhaps it was not resolved in the M^3 data, although Li et al. found there was no bias in the acquisition of M^3 data for these craters that lack detections of surface water ice [12].

Subsurface ice. In addition to surface frost, the lunar poles likely host subsurface ice, as inferred from neutron spectrometer data, the LCROSS experiment, and radiometer measurements [e.g., 13–18]. As mentioned earlier, measurements of polar crater morphometry indicate a shallowing of craters with latitude, suggestive of subsurface ice deposits up to ~50 m thick [1, 2], and large volumes of subsurface ice are consistent with recent Monte Carlo modeling of ice deposition [19].

On Mars, the presence of subsurface ice has been correlated with smooth surface textures on the scales of ~10–100 m [5] and ~0.5–10 km [3, 4]. We suggest subsurface ice may also be responsible for the spatial correlation between low ruggedness indices and ISZs found here. Ongoing work includes analyzing neutron spectrometer data to place constraints on the abundance and burial depth of ice that could potentially be subduing overlying topography.

Conclusions: The distinct correlation between Mode 1 and $T_{max} \leq 112$ K is consistent with the presence of volatiles softening lunar polar topography, although the vertical magnitude of softening implied by the TRIs is only a few meters. This finding is consistent with previous observations that suggest ice does not exist at the lunar surface as thick, pervasive sheets [e.g., 10–12, 20, 21]. The subtle topographic softening observed within ISZs is more consistent with (a) subsurface ices, (b) thin, frosty veneers that drape but do not obscure the underlying regolith topography, or (c) some combination of these. Future exploration of polar craters, especially applying ground-based remote sensing or drilling [e.g., 22], is essential in resolving the presence, form, and abundance of surface and/or subsurface volatiles that may be altering the surface topography.

Acknowledgments: A.N.D. was supported by an appointment to the NASA Postdoctoral Program at Ames Research Center, administered by USRA under contract with NASA.

References: [1] Kokhanov A. A. et al. (2015) *SSR, 49,* 295–302. [2] Rubanenko L. et al. (2019) *Nat Geo, 12,* 597–601. [3] Kreslavsky M. A. and Head J. W. (2000) *JGRP, 105,* 26695–26711. [4] Kreslavsky M. A. and Head J. W. (2002) *GRL, 29,* 14-1–14-4. [5] Putzig N. E. et al. (2014) *JGRP, 119,* 1936–1937. [6] Vasavada A. R. et al. (1999) *Icarus, 141,* 179–193. [7] Williams J.-P. et al. (2019) *JGRP, 124,* 2505–2521. [8] Riley S. J. et al (1999) *IJS, 5,* 23–27. [9] Hobson R. D. (1972) Chorley R. J., *ed.,* 221–245. [10] Hayne P. O. et al. (2015) *Icarus, 255,* 58–69. [11] Fisher E. A. et al. (2017) *Icarus, 292,* 74–85. [12] Li S. et al. (2018) *PNAS, 115,* 8907–8912. [13] Moon S. et al. (2020) *GRL in press,* e2020GL090780. [14] Feldman W. C. et al. (2000) *JGRP, 105,* 4175–4195. [15] Mitrofanov I. G. et al. (2010) *Science, 330,* 483–486. [16] Colaprete A. et al. (2010) *Science, 330,* 463–468. [17] Luchsinger K. M. et al. (2021) *Icarus, 354,* 114089. [18] Yang F. et al. (2019) *AA, 2019,* 3940837. [19] Cannon K. M. et al. (2020) *GRL, 47,* e2020GL088920. [20] Haryuama J. et al. (2008) *Science, 322,* 938–939. [21] Farrell W. M. et al. (2019) *GRL, 46,* 8680–8688. [22] Colaprete A. et al. (2020) *LPS 51,* 2241.